# Experimental Section

## Materials

$Na_2MoO_4 \cdot 2H_2O$ (≥99.5%), $C_4H_4O_6KNa \cdot 4H_2O$ (≥99.9%), NaClO (≥99.9%), $C_9H_{11}NO$ (≥99.5%), $C_5FeN_6Na_2O$ (≥99.0%), $C_{12}H_{14}N_2 \cdot 2HCl$ (≥99.0%), $N_2H_4$ (≥99.9%), $H_2SO_4$ (98%), $NH_4Cl$ (≥99.5%), $SO_2(NH_2)_2$ (≥99.5%), $D_2O$ (≥99.9%) and DMSO (≥99.0%) were purchased from Sigma-Aldrich Chemical Reagent Co., Ltd. B and P powder (≥99.0 wt%), $C_2H_2O_4 \cdot 2H_2O$ (≥99.9%), $C_7H_6O_3$ (≥99.5%), $C_7H_5NaO_3$ (≥99.5%), LiF (≥99.9%), $LiClO_4$ (≥99.9%), HCl (37%) and Nafion (5 wt%) were obtained from Sinopharm Chemical Reagent Co., Ltd.

## Synthesis of BP

BP was synthesized using a reported vacuum-sealed method with a slight modification[1]. Initially, a blend of B and P powders (with a B:P molar ratio of 1:1) with 200 mg was loaded into a silica tube, which was subsequently vacuum-sealed. The silica tube was subsequently subjected to thermal annealing at 1000 $^oC$ for 10 h. Afterwards, the powder was washed with 0.1 M HCl and deionized water to eliminate impurities and obtain BP.

## Electrochemical experiment

Electrochemical performance was investigated with a standard three-electrode system at a CHI-760E electrochemical workstation with each as-prepared catalyst coated on a carbon cloth (CC), a graphite rod and an Ag/AgCl (saturated KCl) as the working, the counter and the reference electrodes, respectively. All potentials were referenced to reversible hydrogen electrode (RHE) by following equation: $E_{RHE}$ (V)=$E_{Ag/AgCl}$+0.198+0.059×pH. The electrocatalytic NORR measurements were conducted within a gas-tight H-cell with NO-saturated 0.5 M $Na_2SO_4$ separated by a Nafion 211 membrane. Before NRR test, the feeding gases were purified using two glass bubblers filled with 4 M KOH solution[2], and the cathodic compartment was purged with Ar for a minimum of 30 minutes to eliminate any remaining oxygen. During the potentiostatic testing, NO flow (99.9%, 20 mL $min^{-1}$) was continuously fed to the cathodic compartment. After electrolysis for 1 h at various potentials, liquid

and gas products were detected by colorimetry and gas chromatography (GC, Shimadzu GC2010), respectively. The detailed procedures were provided in our previous publications[3].

$NH_3$ yield rate and $NH_3$-Faradaic efficiency ($FE_{NH3}$) were calculated by the following equation[4]:

$$NH_3 \text{ yield rate} = (c \times V) / (17 \times t \times A) \quad (1)$$

$$FE_{NH3} = (5 \times F \times c \times V) / (17 \times Q) \times 100\% \quad (2)$$

where $c$ (μg $mL^{-1}$) is the measured $NH_3$ concentration, $V$ (mL) is the volume of electrolyte in the cathode chamber, $t$ (s) is the electrolysis time and $A$ is the surface area of CC (1×1 $cm^2$), $F$ (96500 C $mol^{-1}$) is the Faraday constant, $Q$ (C) is the total quantity of applied electricity.

**Characterizations**

X-ray diffraction (XRD) was performed on a Rigaku D/max 2400 diffractometer. Transmission electron microscopy (TEM) and high-resolution transmission electron microscopy (HRTEM) were performed on a Tecnai $G^2$ F20 microscope. X-ray photoelectron spectroscopy (XPS) analysis was collected on a PHI 5702 spectrometer.

**Calculation details**

Spin-polarized density functional theory (DFT) calculations were performed using the Cambridge sequential total energy package (CASTEP) with projector augmented wave pseudopotentials. The Perdew-Burke-Ernzerhof (PBE) generalized gradient approximation (GGA) functional was used for the exchange-correlation potential. The van der Waals interaction was described by using the empirical correction in Grimme's scheme (DFT+D). During the geometry optimization, the convergence tolerance was set to be $1.0 \times 10^{-5}$ eV for energy and 0.02 eV $Å^{-1}$ for force. The electron wave functions were expanded using plane waves with a cutoff energy of 500 eV. The 4 × 4 × 1 Monkhorst-Pack mesh was used in Brillouin zone sampling. BP (111) was modeled by a 3 × 3 supercell, and a vacuum region of 15 Å was used to separate adjacent slabs.

The adsorption energy (ΔE) is defined as

$$\Delta E = E_{ads/slab} - E_{ads} - E_{slab} \quad (3)$$

where $E_{ads/slab}$, $E_{ads}$ and $E_{slab}$ are the total energies for adsorbed species on slab, adsorbed species and isolated slab, respectively.

The Gibbs free energy (ΔG, 298 K) of reaction steps is calculated by

$$\Delta G = \Delta E + \Delta ZPE - T\Delta S \quad (4)$$

where $\Delta E$ is the adsorption energy, $\Delta ZPE$ is the zero-point energy difference and $T\Delta S$ is the entropy difference between the gas phase and adsorbed state.

Molecular dynamics (MD) simulations were performed using a force field type of Universal. The electrolyte system was geometrically optimized by setting the convergence tolerance of $2.0\times10^{-5}$ kcal/mol for energy and 0.001 kcal/mol/Å for force. The non-bond interaction was processed by Ewald with accuracy of $10^{-5}$ Kcal/mol and the repulsive cutoff was chosen as 12 Å. The electrolyte system was set up by randomly placing 1000 $H_2O$, 50 H and 50 NO molecules in the simulation box. After geometry optimization, the MD simulations were performed under the universal field with the total simulation time of 500 ps at a time step of 1 fs.

The radial distribution function (RDF) is calculated as

$$g(r) = \frac{dN}{4\pi\rho r^2 dr} \quad (5)$$

where $dN$ is the amount of NO/H in the shell between the central particle $r$ and $r+dr$, $\rho$ is the number density of NO/H.

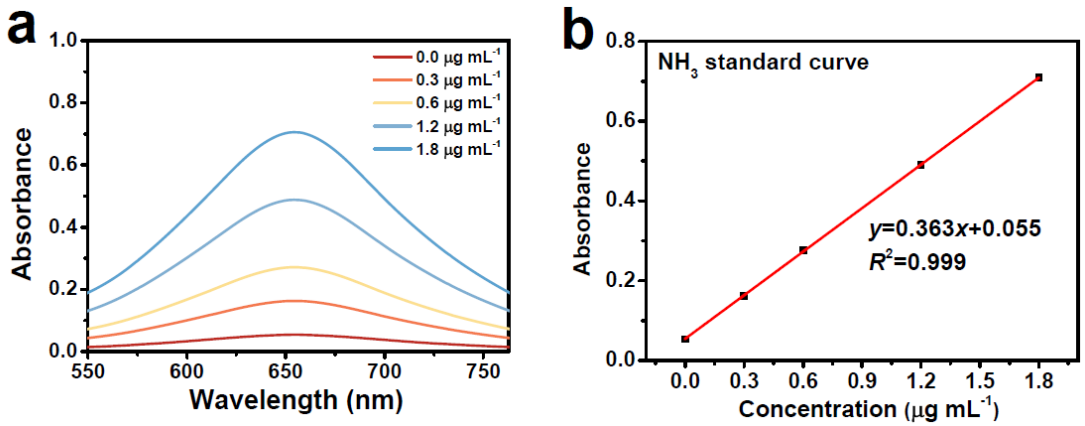


Fig. S1. (a) UV-vis absorption spectra of $NH_4Cl$ assays after incubated for 2 h at ambient conditions. (b) Calibration curve used for the calculation of $NH_3$ concentrations.

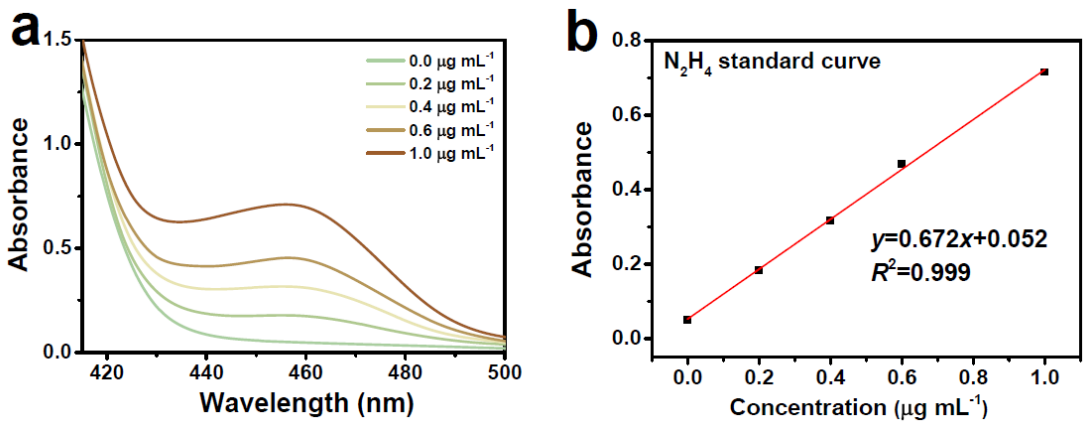


Fig. S2. (a) UV-vis absorption spectra of $N_2H_4$ assays after incubated for 20 min at ambient conditions. (b) Calibration curve used for calculation of $N_2H_4$ concentrations.

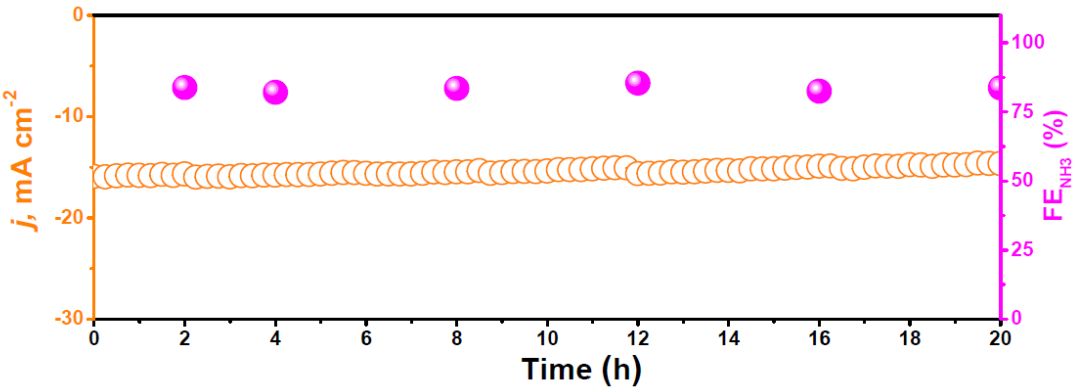


Fig. S3. Long-term chronoamperometry test of BP for 20 h at -0.7 V.

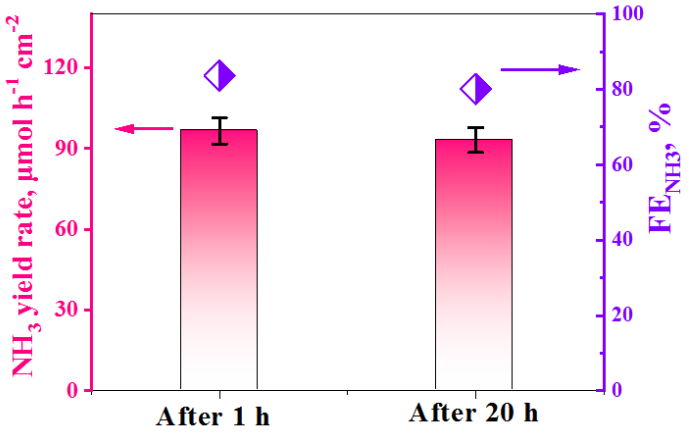


Fig. S4. $NH_3$ yield rates and $FE_{NH3}$ of BP after 1 h and 20 h electrolysis.

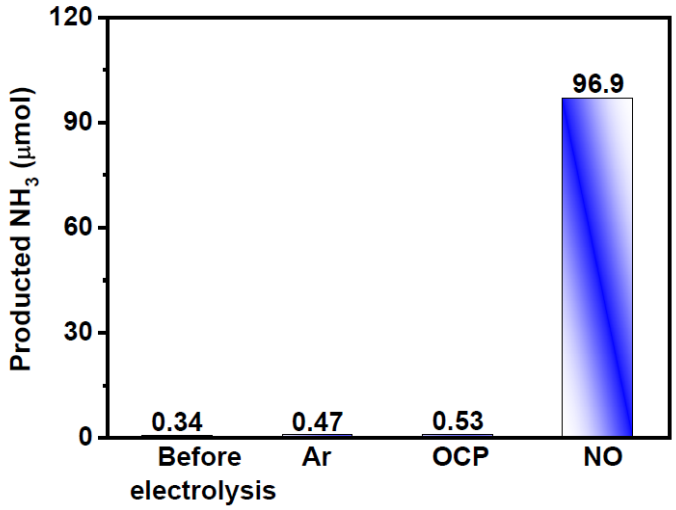


Fig. S5. Amounts of produced $NH_3$ over BP under different conditions at -0.7 V.

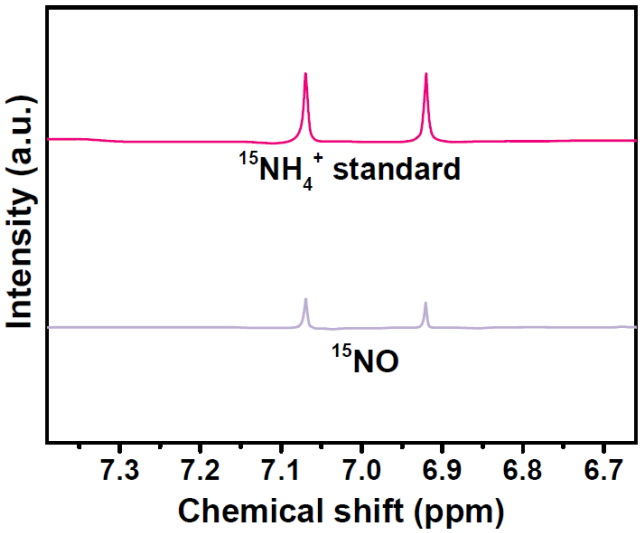


Fig. S6. $^{1}H$ NMR spectra of $^{15}NH_4^+$ standard sample and that fed by $^{15}NO$ after NORR electrolysis on BP for 1 h at -0.7 V.

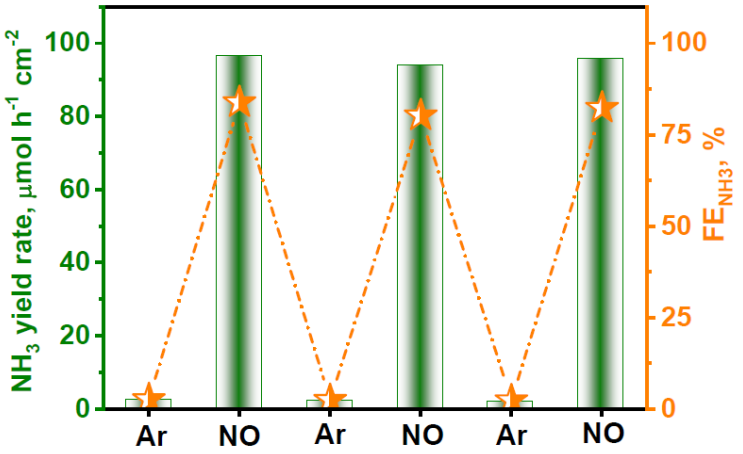


Fig. S7. NO-Ar gas switching experiment on BP at -0.7 V.

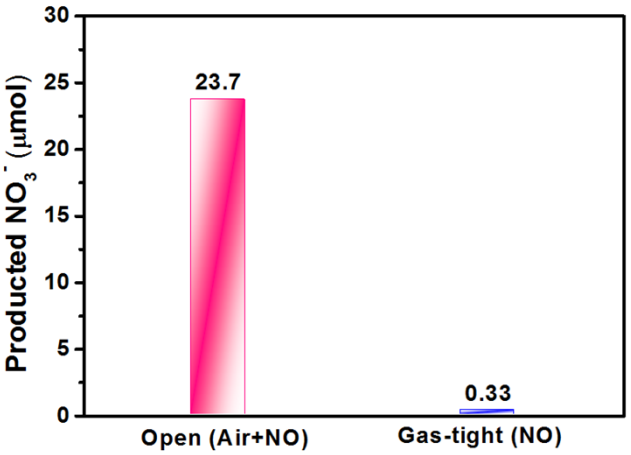


Fig. S8. Amounts of produced $NO_3^-$ in open and gas-tight electrolytic cells.

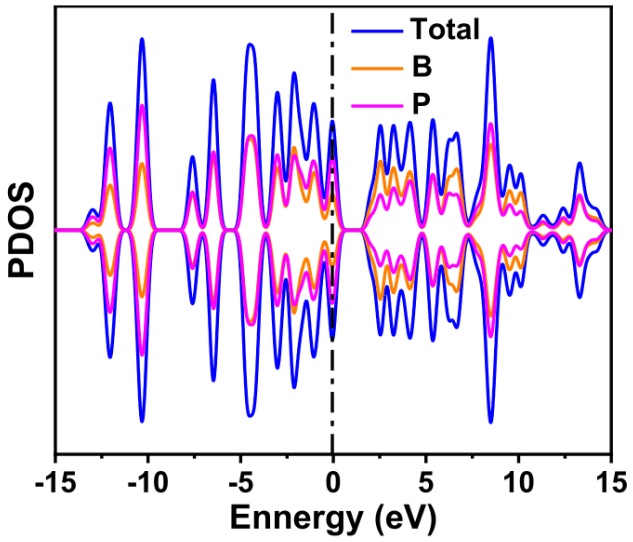


Fig. S9. DOS profile of BP.

The narrow band gap of BP and its occupied state near the Fermi level are indicative of the high electron transport capability of BP.

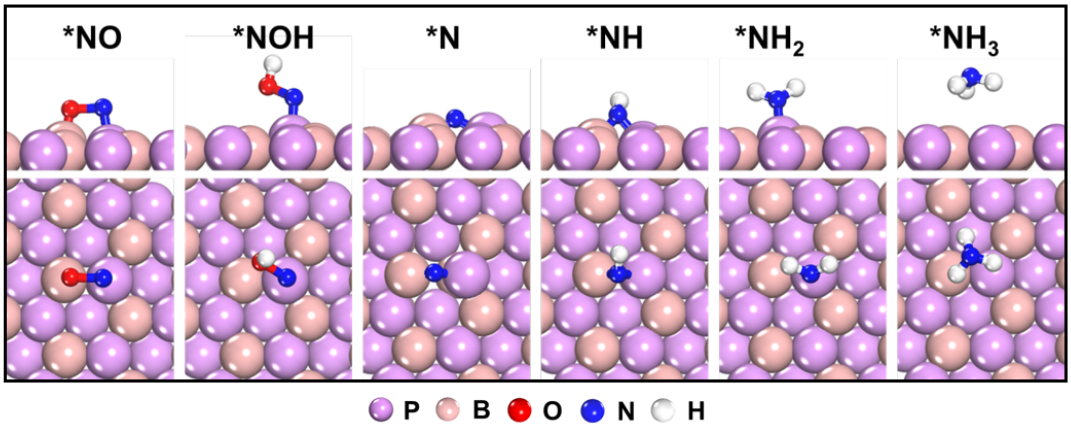


Fig. S10. Optimized structures of the reaction intermediates through the NOH pathway on BP.

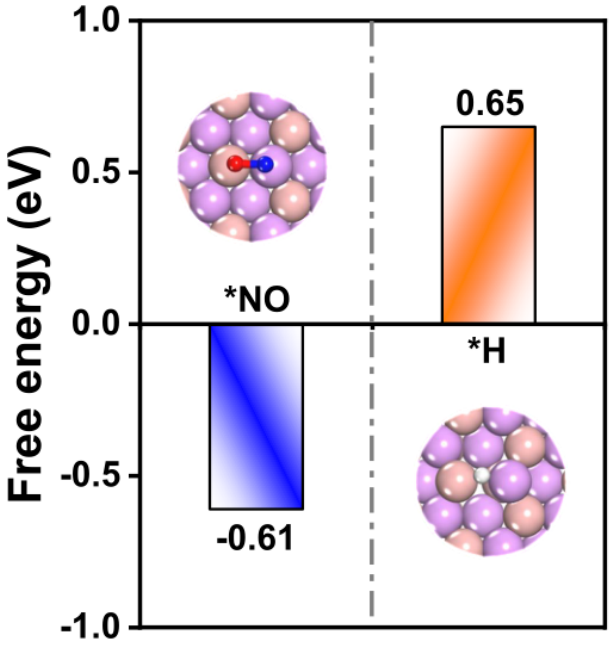


Fig. S11. Comparison of the *H/*NO binding free energies on BP.

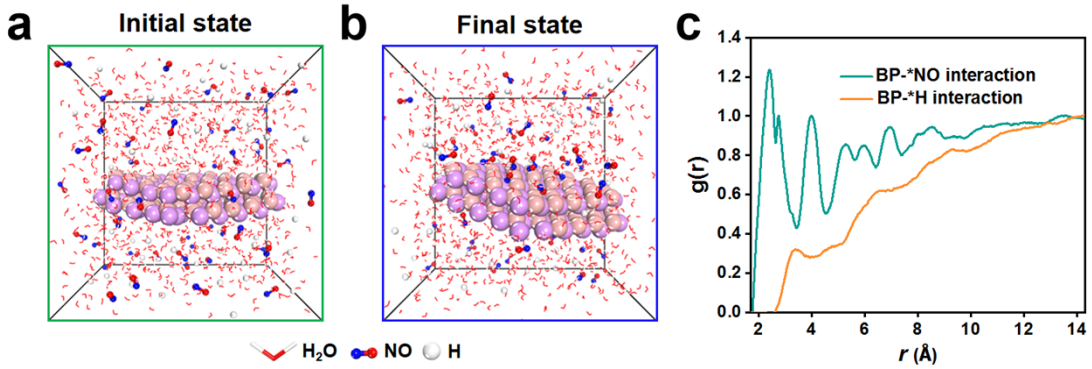


Fig. S12. (a, b) Snapshots of the (a) initial state and (b) final state for the dynamic process of NO and H adsorption on BP after MD simulations, and corresponding (c) RDF curves.

As seen, before the simulation, NO/H are uniformly distributed in the electrolyte systems (Fig. S12a). After simulations, relatively more NO coverage than H can be observed on BP (Fig. S12b), and the corresponding radial distribution function (RDF, Fig. S12c) curves display a higher g(r) value related to BP-*NO interaction compared to BP-*H interaction, further corroborating the high NORR selectivity of BP against HER.

Table S1. Comparison of the optimum $NH_3$ yield and $NH_3$-Faradic efficiency ($FE_{NH3}$) for recently reported state-of-the-art NORR electrocatalysts at ambient conditions.

| Catalyst | Electrolyte | $NH_3$ yield rate ($\mu mol\ h^{-1}\ cm^{-2}$) | $FE_{NH3}$ (%) | Potential (V vs. RHE) | Ref. |
|---|---|---|---|---|---|
| NiFe-LDH | 0.25 M $Li_2SO_4$ | 112 | 82 | -0.7 | [5] |
| Ni@NC | 0.1 M HCl | 34.6 | 72.3 | 0.16 | [6] |
| RuGa | 0.1 M $K_2SO_4$ | 160.3 | 72.3 | -0.2 | [7] |
| $Cu_2O$@$CoMn_2O_4$ | 0.1 M $Na_2SO_4$ | 94.18 | 75.05 | -0.9 | [8] |
| $CoS_{1-x}$ | 0.2 M $Na_2SO_4$ | 44.67 | 53.62 | -0.4 | [9] |
| $MnO_{2-x}$ NA/TM | 0.2 M $Na_2SO_4$ | 9.9 | 82.8 | -0.7 | [10] |
| $MoS_2$/GF | 0.1 M HCl | 99.6 | 76.6 | 0.1 | [11] |
| $Ni_2P$/CP | 0.1 M HCl | 33.47 | 76.9 | -0.2 | [12] |
| $Ru_{0.05}Cu_{0.95}$ | 0.05 M $Na_2SO_4$ | 17.68 | 64.9 | -0.5 | [13] |
| NiO/TM | 0.1 M $Na_2SO_4$ | 125.3 | 90 | -0.6 | [14] |
| FeP/CC | 0.2 M PBS | 85.62 | 88.49 | -0.2 | [15] |
| Bi NDs | 0.1 M $Na_2SO_4$ | 70.2 | 89.2 | -0.5 | [16] |
| **BP** | **0. 5 M $Na_2SO_4$** | **96.6** | **83.8** | **-0.7** | **This work** |

## Supplementary references


[1]. S. Mou, T. Wu, J. Xie, Y. Zhang, L. Ji, H. Huang, T. Wang, Y. Luo, X. Xiong and B. Tang, *Adv. Mater.*, 2019, **31**, 1903499.

[2]. L. Zhang, J. Liang, Y. Wang, T. Mou, Y. Lin, L. Yue, T. Li, Q. Liu, Y. Luo, N. Li, B. Tang, Y. Liu, S. Gao, A. A. Alshehri, X. Guo, D. Ma and X. Sun, *Angew. Chem. Int. Edit.*, 2021, **60**, 25263-25268.

[3]. Y. Luo, K. Chen, P. Shen, X. Li, X. Li, Y. Li and K. Chu, *J. Colloid Interf. Sci.*, 2023, **629**, 950-957.

[4]. Y. Wang, C. Wang, M. Li, Y. Yu and B. Zhang, *Chem. Soc. Rev.*, 2021, **50**, 6720-6733.

[5]. G. Meng, T. Wei, W. Liu, W. Li, S. Zhang, W. Liu, Q. Liu, H. Bao, J. Luo and X. Liu, *Chem. Commun.*, 2022, **58**, 8097-8100.

[6]. S. Sethuram Markandaraj, T. Muthusamy and S. Shanmugam, *J. Adv. Sci*, 2022, **9**, 2201410.

[7]. H. Zhang, Y. Li, C. Cheng, J. Zhou, P. Yin, H. Wu, Z. Liang, J. Zhang, Q. Yun and A. L. Wang, *Angew. Chem. Int. Edit.*, 2022, e202213351.

[8]. C. Bai, S. Fan, X. Li, Z. Niu, J. Wang, Z. Liu and D. Zhang, *Adv. Funct. Mater.*, 2022, **32**, 2205569.

[9]. L. Zhang, Q. Zhou, J. Liang, L. Yue, T. Li, Y. Luo, Q. Liu, N. Li, B. Tang, F. Gong, X. Guo and X. Sun, *Inorg. Chem.*, 2022, **61**, 8096-8102.

[10]. Z. Li, Z. Ma, J. Liang, Y. Ren, T. Li, S. Xu, Q. Liu, N. Li, B. Tang, Y. Liu, S. Gao, A. A. Alshehri, D. Ma, Y. Luo, Q. Wu and X. Sun, *Mater. Today Phys.*, 2022, **22**, 100586.

[11]. L. Zhang, J. Liang, Y. Wang, T. Mou, Y. Lin, L. Yue, T. Li, Q. Liu, Y. Luo, N. Li, B. Tang, Y. Liu, S. Gao, A. A. Alshehri, X. Guo, D. Ma and X. Sun, *Angew. Chem. Int. Ed.*, 2021, **133**, 25467-25472.

[12]. T. Mou, J. Liang, Z. Ma, L. Zhang, Y. Lin, T. Li, Q. Liu, Y. Luo, Y. Liu, S. Gao, H. Zhao, A. M. Asiri, D. Ma and X. Sun, *J. Mater. Chem. A*, 2021, **9**, 24268-24275.

[13]. J. Shi, C. Wang, R. Yang, F. Chen, N. Meng, Y. Yu and B. Zhang, *Sci. China Chem.*, 2021, **64**, 1493-1497.

[14]. P. Liu, J. Liang, J. Wang, L. Zhang, J. Li, L. Yue, Y. Ren, T. Li, Y. Luo, N. Li, B. Tang, Q. Liu, A. M. Asiri, Q. Kong and X. Sun, *Chem. Commun.*, 2021, **57**, 13562-13565.

[15]. J. Liang, Q. Zhou, T. Mou, H. Chen, L. Yue, Y. Luo, Q. Liu, M. S. Hamdy, A. A. Alshehri, F. Gong and X. Sun, *Nano Res.*, 2022, **15**, 4008-4013.

[16]. Y. Lin, J. Liang, H. Li, L. Zhang, T. Mou, T. Li, L. Yue, Y. Ji, Q. Liu, Y. Luo, N. Li, B. Tang, Q. Wu, M. S. Hamdy, D. Ma and X. Sun, *Mater. Today Phys.*, 2022, **22**, 100611.